Low cost environmentally benign porous paper based fuel cells for micro-nano systems[†]

Sweta Lal,[‡] Vinod M. Janardhanan,[*,‡] Melepurath Deepa,[*,¶] Anand Sagar,[‡] and Kirti Chandra Sahu[*,‡]

Department of Chemical Engineering, Indian Institute of Technology Hyderabad, Kandi, 502 285, and Department of Chemistry, Indian Institute of Technology Hyderabad, Kandi, 502 285

E-mail: vj@iith.ac.in; mdeepa@iith.ac.in; ksahu@iith.ac.in

Phone: +91 (0)40 2301 6073. Fax: +91 (0)40 2301 6032

Abstract

This work deals with the development of a paper based fuel cell for application in micro-nano systems. In this cell, a porous paper serves as a transport medium and eliminates the need for any metering devices that are integral to conventional fuel cells. Since only very small flow rates of reagents can be achieved on paper, these cells produce only a few milli-watts of power. In this work, formic acid is used as the fuel and potassium permanganate is used as the oxidant. Since the cell presented here is membraneless, both formic acid and potassium permanganate are mixed with sulfuric acid, and they form the anolyte and the catholyte, respectively. A special cell geometry has been designed and implemented to minimize and delay the fuel and oxidant cross over effects. In order to keep the cost low, graphite sheets without

[†]patent application based on the results presented here has been filed through Indian Institute of Technology Hyderabad, India (Application number: 3515/CHE/2015).

[*]To whom correspondence should be addressed

[‡]Department of Chemical Engineering, Indian Institute of Technology Hyderabad, Kandi, 502 285

[¶]Department of Chemistry, Indian Institute of Technology Hyderabad, Kandi, 502 285

any metal loading are used as the current collectors. Two variants of filter paper are used for implementing the fuel cells. Cell characterization is accomplished by performing detailed potentiometric and impedance studies. Our study on formic acid cell shows that the porous paper cell architecture can be extended to other fuel-oxidant combinations as well.

Introduction

Cost-effective and eco-friendly power sources for single use diagnostic devices or micro-nano systems (MNSs) are expected to have a tremendous impact on rural health care, environmental monitoring and communications technology. Nano-watts to milli-watts of power is adequate enough to run these devices.[1,2] Single use diagnostic devices presently use battery activated optical sensors,[2–4] which are discarded after usage. Substituting these small power sources with environmentally safe micro fuel cells is a practical solution. Generally, fuel cells, including the ones that rely on microfluidics for smooth operation, need a metering device which ensures a continuous flow of the fuel and the oxidant through the channels. By removing the metering device from the fuel cell assembly, significant advancements can be realized in the micro-fuel-cell technology, and in particular, its application to biomedical devices and MNSs. In this context, in a few recent works, porous paper has been deployed as a transport medium for self-metering of liquid fuels. The inherent physical properties of paper, such as porosity and capillary action allow an unobstructed transport of liquids through the micro channels of the paper. This innate property of paper has lately been used to develop fuel cells which are useful for biosensing applications.[4] Paper based chemiluminescence biosensors for the simultaneous detection and quantification of glucose and uric acid in artificial urine have already been demonstrated.[5] Other useful features of paper based sensing devices or fuel cells are low cost, ease of use and disposal, and low consumption of reagents. Therefore, paper based fuel cells are viable alternatives to battery operated MNSs for the former are not only

cheap, but are also made up of less toxic components.

Since the flow of the fuel and oxidant through paper is laminar due to low flow rate, it is ideal for developing membraneless fuel cells. In these cells, the ionic transport between the electrodes is achieved by adding electrolyte to both fuel and oxidant streams, which are called the anolyte and catholyte, respectively. The mixing of anolyte and catholyte is confined to a liquid-liquid interface, which acts as a virtual membrane through which charge transport occurs. Although laminar flow prevents convective mixing of anolyte and catholyte, in paper, eventual mixing of reagents will occur due to the non-directionality associated with cellulose fibre orientation and the randomness of pore networks. The degree of transverse mixing due to diffusion depends on the Péclet number (Pe=$Q/\mathcal{D}$), wherein Q and $\mathcal{D}$ denote the volumetric flow rate and diffusivity, respectively; thus a large value of Pe would limit the diffusional mixing.[6,7] An extensive review on laminar flow membraneless fuel is provided by Shaegh et al.[7]

Since paper based cells operate at room temperature, only fuels that undergo electrochemical oxidation at room temperature can be used. Formic acid (HCOOH) and methanol (CH_3OH) have gained significant interest in the recent past as direct fuels for use in low temperature fuel cells[8–15] (e.g. Proton exchange membrane fuel cells (PEMFCs), which typically function in the range of 80° - 120°). Nevertheless, these can also be used in fuel cells that operate at room temperature.[4,11] Therefore they have been the most commonly used liquid fuels for laminar flow membraneless fuel cells.[7] Pure formic acid has a volumetric energy density of 2.08 kWh/l[10] and that of methanol is 4.69 kWh/l,[10] both of which are higher than that of liquid hydrogen and are good sources of hydrogen. Although the volumetric energy density is higher for CH_3OH, the theoretical open circuit potential of the $HCOOH/O_2$ system is 1.45 V, which is higher than that of the CH_3OH/O_2 system (1.2 V). Moreover, formic acid being a proton conductor, also serves as a strong electrolyte for the transport of protons.[9]

Generally Pt or Pd or Au have been used as catalysts in anode in direct formic acid fuel

cells. The use of expensive noble metals can not be justified for use in MNSs or in single use diagnostics devices that are disposed after use. What is required is a cell that is made of cheap components; however, without any additional components such as metering devices that would make the system more complex. In this work, we present a novel direct formic acid fuel cell operating at room temperature, using paper as the transport medium and graphite as electrodes without incorporating any catalysts. As discussed earlier, the use of paper eliminates the need for metering devices. The cell assembly, anolyte and catholyte preparation and the electrochemical characterization and analysis are described below.

Experimental procedure

A schematic representation of the experimental set up is shown in Fig. Figure 1. A filter

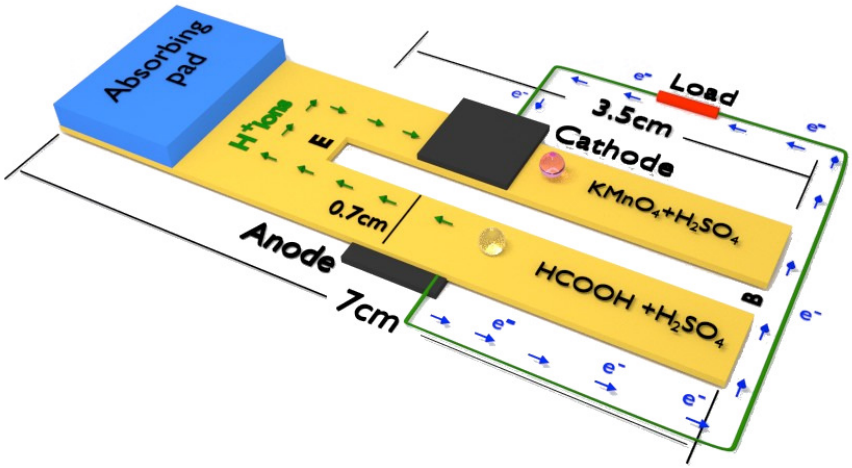

Figure 1: Schematic (not to scale) representation of the experimental cell configuration. **E** represents the end of the slit and **B** represents the beginning of the slit. The green arrows show the direction of transport of H^+ ions and blue arrows show the direction of electron transport.

paper serves as the medium for the transport of anolyte and catholyte. The paper is cut into a 7 cm long strip having a width of (1.4+d_s) cm, where d_s is the slit width which is

varied. At one extreme end of the strip, an absorbing pad made of tissue paper is attached to absorb the anolyte and catholyte. The graphite electrodes (13 mm $\times$ 5 mm $\times$ 1.3 mm) are placed on either side of the strip, and these two electrodes are separated by a thin slit. The slit prevents the direct mixing of anolyte and catholyte, although, mixing due to diffusion occurs at the end of the slit. This position is designated by the letter '**E**' in Fig. Figure 1. The contact area between the electrodes and filter paper is 0.35 cm^2. The graphite sheet at the anode faces down and the cathode faces open air. Since the cathode is porous and open to the atmosphere, it allows air to diffuse into the interface between the paper and graphite electrode. Although the anode faces downwards, a limited diffusion of air can occur at the anode as well. The whole set up is placed on a micro-slide glass plate. The anolyte is prepared by mixing formic acid with H_2SO_4 (4 M) and the catholyte is prepared by mixing potassium permanganate ($KMnO_4$, 1 M) with H_2SO_4 (4 M); all in ultra pure water. Formic acid (100%) and $KMnO_4$ (98.5%) are purchased from Merck and H_2SO_4 (90%) is purchased from Fischer Scientific. Different concentrations of formic acid have been used (6 M-12 M) to identify the optimum concentration of formic acid on the basis of best electrochemical performance. Additionally, the position of the electrodes from the end of the slit '**E**' and width of the slit d_s are also varied to determine the effect of electrode positioning and slit width on the performance of the system. Since graphite is a good inexpensive conductor of electrons, other current collectors were not used.

The self-transportation of anolyte and catholyte has been achieved by dipping the two tail ends of the strip (or beginning of the slit marked by '**B**' in Fig. Figure 1) into separate reservoirs of the anolyte and the catholyte. Since, the rate of flow strongly depends on the nature of the filter paper, two different filter papers (Whatmann and Raveria) are used in this study, and both allows very slow transportation of fluids to the respective electrodes. In order to speed up the measurements, droplets of anolyte and catholyte are manually dropped near the electrodes. Droplets are never discharged directly on the electrodes as it may disturb the system. The dc polarization and the impedance measurements are

performed using Autolab

Results and discussion

The half cell reactions occurring at the anode and cathode respectively are

$$\mathrm{HCOOH} \rightleftharpoons 2\mathrm{H}^{+} + 2\mathrm{e}^{-} + \mathrm{CO}_2 \quad (E^0 = -0.25\ V), \tag{1}$$

and

$$\mathrm{MnO_4}^{-} + 8\mathrm{H}^{+} + 5\mathrm{e}^{-} \rightleftharpoons \mathrm{Mn}^{2+} + 4\mathrm{H_2O} \quad (E^0 = 1.51\ V). \tag{2}$$

The overall reaction in the cell is given by

$$5\mathrm{HCOOH} + 2\mathrm{MnO_4}^{-} + 6\mathrm{H}^{+} \rightleftharpoons 2\mathrm{Mn}^{2+} + 8\mathrm{H_2O} + 5\mathrm{CO_2}. \tag{3}$$

The concentration gradient of the protons and the voltage difference between the anode and cathode leads to the transport of protons from the anode to the cathode. Simultaneously, electrons move from the anode to the cathode via the external circuit. Two different mechanistic pathways have been proposed in the literature for the oxidation of formic acid. One pathway assumes a multiple electron transfer reaction and the other pathway assumes single electron transfer with the formation of CO as an intermediate product. The formation of CO is favored when Pt or Pd is used as a catalyst. Irrespective of the pathway, the oxidation potential for HCOOH is -0.25 V. At the cathode, $KMnO_4$ dossociates to form K^+ and MnO_4^- ions. The MnO_4^- ions react with H^+ to form H_2O and the reduction potential for this reaction at the cathode is 1.51 V. The overall cell reaction gives an open circuit voltage (OCV) of 1.76 V.

The slit introduced in the strip between the graphite electrodes restricts the direct mixing of the fuel and the oxidant to a great extent. The variation of OCV with time for different concentrations of formic acid in cells with electrodes placed at a location 2 cm

away from the end of the slit for Whatmann filter paper (40, ashless, diameter-150mm, purchased from Hychem, Inc.) is shown in Fig. Figure 2. It can be seen that the value of OCV decreases slightly with time for all concentrations of formic acid considered in this study, i.e 6 M, 8 M, 10 M, and 12 M. A number of experiments have been performed and Fig. Figure 2 shows only a representative sample. The maximum variation in OCV for each formic acid concentration across all experiments with the electrodes placed 2 cm away from the end of the slit is approximately ± 0.15 V. In Fig. Figure 2, the OCV decreases with time, which is essentially caused by (a) the eventual fuel and oxidant crossover, and (b) the fuel and oxidant dilution effect; factors which are detrimental to the electrochemical performance of the fuel cell. The overall cell reaction leads to the formation of CO_2 at the anode and H_2O at the cathode. Ideally the CO_2 evolved at the anode must diffuse out of the liquid phase. However, since the anode is kept below the paper strip, CO_2 can get trapped and this will lead to poor contact between the paper and the electrode.[16] Similarly the formation of H_2O at the cathode can further dilute $KMnO_4$. All these effects lead to the gradual loss in OCV. The average rate of drop of OCV for cell employing 8 M formic acid is 0.0051 V/min. For other concentrations of the formic acid, the OCV decline rate was found to lie in the range of 0.0025 to 0.0082 V/min. A comparison between the OCV generated by cells made of Whatmann and Riveria filter papers are shown in Fig. Figure S1 and the performance comparison is shown in Fig. Figure S2. The difference in performance between the two papers is due to the micro-structural difference which is shown in Fig. Figure S3. Since Whatmann filter paper lead to better performance compared to Riveria under identical conditions, the rest of the experiments are performed using Whatmann filter paper.

The width of the slot and the positioning of the graphite electrodes from the end of the slit 'E' plays a key role in determining the diffusion path length of the ions. If the distance between the electrodes is long, the diffusion path length for the ions that are released at the anode to reach the cathode is enhanced, thus leading to larger Ohmic losses in the system.

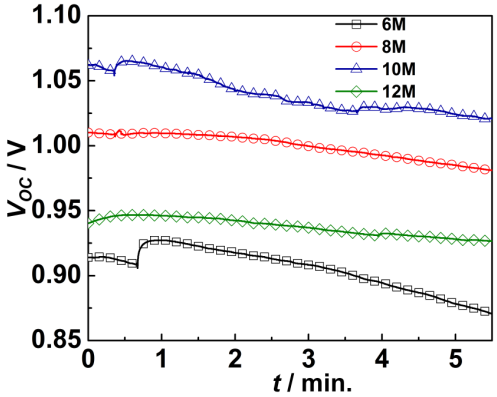

Figure 2: Open circuit voltage for different formic acid concentrations. The electrodes are placed 2 cm away from the end of the slit

Similar is the effect while increasing the slit width. The effect of electrode positioning from the end of the slit on the cell performance is shown in Fig. Figure 3 and the corresponding power density is shown in Fig. Figure 4.

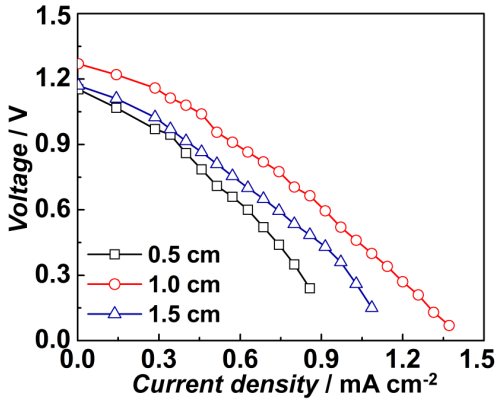

Figure 3: Variation in cell voltage as a function of current density for different electrode positions from the end of the slit for 8 M formic acid

It is evident from these figures that the cell performance is lower when the electrode position is too close or too away from the end of the slit. When the electrodes are placed too close to the end of the slit, the fuel and oxidant crossover to the opposite electrodes, which in turn adversely affect the cell performance. On the other hand, when the electrodes are placed far away from the slit end, the Ohmic losses due to the longer path of ion transport leads to the drop in cell performance. Since for each experiment, a new cell is used, slight variations in OCV are observed between different runs, and the maximum difference is

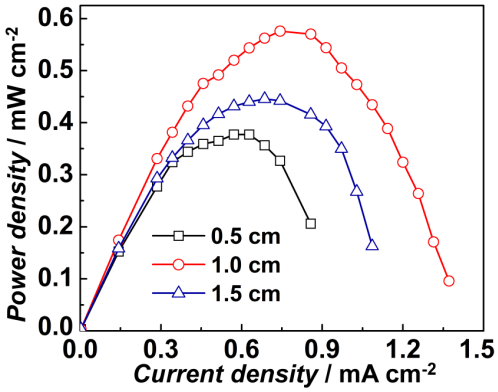

Figure 4: Variation in cell power density as a function of current density for different electrode positions from the end of the slit for 8 M formic acid

of the order of ± 0.2 V. Variations in room temperature and humidity are also found to influence the cell performance slightly. Therefore, the room temperature is controlled by an air-conditioner, which maintained the room temperature at 24 ^{o}C. Theoretically, one would expect the same OCV in Fig. Figure 3 for all electrode positions, since the Ohmic losses are completely insignificant at open circuit conditions. However, there are slight variations in the experimentally measured OCVs, and we believe that the observed differences are due to the reasons discussed above. Similarly the effect of slit width on cell performance is shown in Fig. Figure 5. It can be clearly seen that the cell performance at 4 mm slit width is superior to the other slit widths considered in this study. Based on the observations made from Fig. Figure 3, Fig. Figure 4, and Fig. Figure 5 for the rest of the experiments the slit width and position of the electrodes from the end of the slit 'E' are maintained at 4 mm and 1 cm respectively.

The polarization behavior of the cells for different formic acid concentrations is displayed in Fig. Figure 6 and Fig. Figure 7. It is evident that the best cell performance is observed for the cell with 8 M formic acid and the I$-$V characteristics at 8 M are found to be almost linear (see Fig. Figure 6) above 0.3 mA/cm^2. The OCV of the cell at 8 M formic acid concentration is $\sim$1.3 V and the cell delivered a maximum power density of 0.57 mW/cm^2 corresponding to a cell voltage of 0.77 V (Fig. Figure 7). Considering that

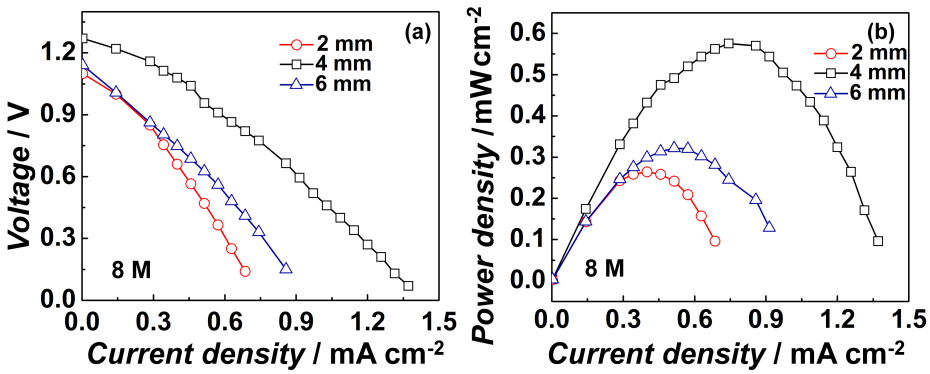

Figure 5: Cell performance at different slit widths using 8M formic acid. The electrodes are placed 1 cm away from the end of the slit 'E'

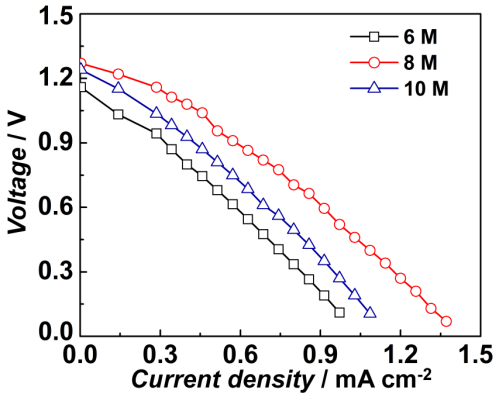

Figure 6: Variation in cell voltage as a function of current density for cells based on different formic acid concentrations. The electrodes are placed 1 cm away from the end of the slit 'E'

the graphite electrodes used here do not employ any catalysts, these results are highly encouraging. However, the obtained OCVs are much lower than the theoretically expected value of 1.76 V. The decrease in OCV from the theoretical value can be attributed to several factors, such as fuel cross over to the cathode, fuel and oxidant flow rates, and the rate of removal of H_2O and CO_2 bubbles, and the pH of the fuel and the oxidant.[7] Since paper is highly absorbing, any H_2O produced as a result of reduction reaction will be absorbed and will cause the dilution of the oxidant. CO_2 formation at the anode and its' accumulation may also contribute to the decrease in OCV from the theoretical value according to Nernst equation. Furthermore, the three phase interface at the anode is accessible to air and hence depending on the oxygen partial pressure, to some extent, the unwanted direct oxidation of formic acid can also occur at the anode. Mn^{2+} formation at the cathode (graphite)/oxidant

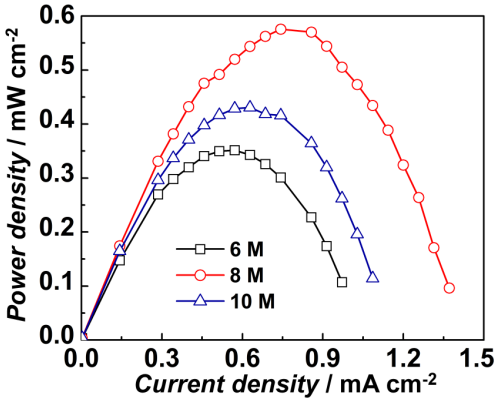

Figure 7: Variation in power density as a function of cell current for cells operating at different formic acid concentrations. The electrodes are placed 1 cm away from the end of the slit 'E'

interface can also impede the reduction process at the cathode. Thus the decrease in OCV obtained for the cell with optimised configuration and fuel concentration, from the theoretical value and its' drop with time are due to several factors. Although the presence of the slit eliminates a long mixing zone, which is typically unavoidable in the 'Y' shaped configuration, a small mixing zone is still present at the end of the slit in the cells under consideration. Thus the presence of the slit delays the fuel and the oxidant crossover to the opposite electrodes, but does not completely eliminate it.

The decrease in cell performance above a certain concentration of formic acid is observed in other direct formic acid fuel cells as well.[9,10] All the factors that lead to the drop in OCV from its' theoretical value are responsible for the lower than the expected performance of the polarized cell. At lower concentrations, the transport of formic acid at the anode limits the cell performance. For higher concentrations of formic acid, faster cross over of formic acid to the cathode and loss of active area due to CO_2 formation are the main reasons for the poor performance of the cell. Since the concentration of the oxidant is kept constant, it is inferred that the the anodic processes limit the cell performance.

The electrochemical impedance measurement of the cells is carried out in the frequency range of 1 MHz to 0.1 Hz at OCV by applying 10 mV sinusoidal perturbation. The Nyquist plots for cell responses at different formic acid concentrations at OCV are

shown in Fig. Figure 8. All the plots exhibit typical depressed semicircle behavior due to frequency dispersion. Except for the cell with 6 M formic acid (Fig. Figure 8(a)), for all other concentrations of formic acid, the Warburg impedance component is observed at low frequencies. In Fig. Figure 8, panels (b)-(d) show a very limited frequency region over which mass transfer effect is present and this is insignificant as compared to the frequency region over which charge transfer resistance is present. Although the low frequency intercept is not well resolved, the charge transfer resistance of the cell slightly increases with the increase in the formic acid concentration with a moderate difference between 10 M and 12 M formic acid concentrations. Since the electro-oxidation of formic acid is a very slow process,[7] significant activation losses can be expected at the anode. The dominance of charge transfer resistance over the Warburg impedance also indicates that the kinetics of the electrode reaction is rather sluggish. Since the oxidant concentration is maintained constant across all experiments, the changes in charge transfer resistances are induced by the variation of formic acid concentration and hence the electrochemical kinetics at the anode. Since the impedance measurements are made at OCV by applying a small amplitude (10 mV) sinusoidal perturbation, the activation over potential will be small and the current response will be linear. Under such conditions, the charge transfer resistance R_{ct} is related to the exchange current density according to,

$$R_{\mathrm{ct}} = \frac{RT}{n_{\mathrm{e}} F i_0}, \tag{4}$$

which leads to an exchange current density of 10^{-2} mA cm^{-2} for the cell with 8 M formic acid concentration. The high frequency resistance also varies slightly with the formic acid concentration.

The impedance response of the cell at 0.77 V with 10 mV amplitude sinusoidal perturbation in the frequency range of 1 MHz to 0.1 Hz is shown in Fig. Figure 9. The voltage of 0.77 corresponds to the maximum power density delivered by 8M formic acid using

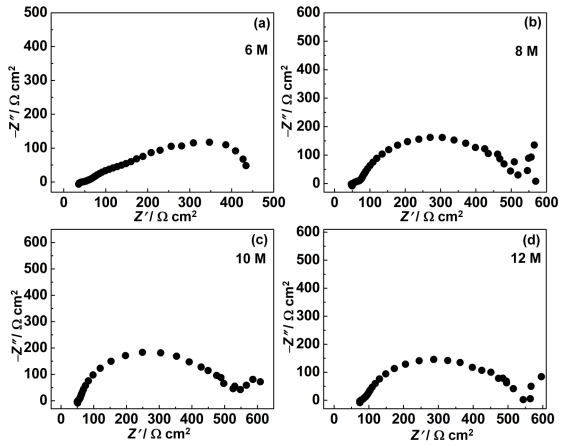

Figure 8: Nyquist plots of the cells with different formic acid concentrations. The relaxation frequencies observed for 6 M, 8 M, 10 M, and 12 M are 37.27 Hz and 0.372 Hz, 7.94 Hz, 10 Hz, 13.89 Hz, respectively. Note that two relaxation frequencies are observed for 6 M formic acid concentration.

Whatman filter paper (Fig. Figure 7). Although not very distinct two semicircles can be observed in Fig. Figure 9. The high frequency intercept (R_{Ω}=59.68 Ωcm^2) is comparable with the Ohmic resistance of the cell at open circuit conditions, however, the charge transfer resistance (R_{ct}=1000 Ωcm^2) is much higher at part load condition. Typically the polarization resistance should decrease when the cell is partly loaded. Therefore, the increased polarization resistance here is probably due to CO_2 accumulation at the anode. Similar to the cell response at OCV, here also mass transfer limitation is present over a very limited range near the low frequency.

The variation of Ohmic resistance of the cells with formic acid concentration is shown in Fig. Figure 10. As the concentration of formic acid increases, the Ohmic resistance of the cell also increases. When concentrated formic acid is used in cells with a membrane, particularly based on membrane electrode assemblies that require to be maintained in the hydrated state, the high frequency resistance increases due to membrane dehydration.[10] This major drawback is eliminated in the case of a membraneless configuration, such as the one presented here. Nevertheless, even in this membraneless configuration, the high frequency resistance increases with formic acid concentration, a behaviour similar

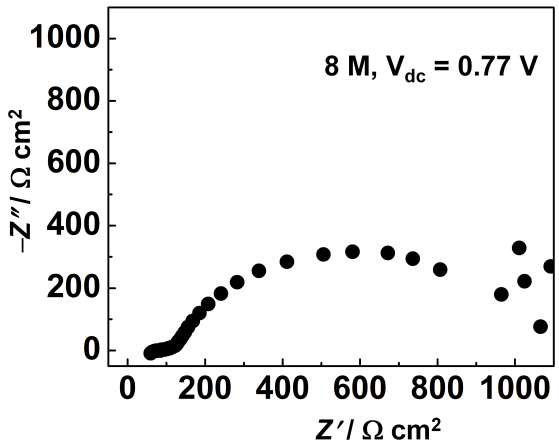

Figure 9: Nyquist plot showing the impedance response of the cell at 0.77 V using 8M formic acid on Whatman filter paper.

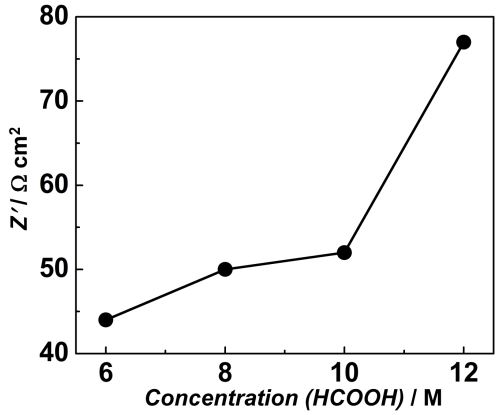

Figure 10: Variation of Ohmic resistance of the cells as a function of formic acid concentration.

to the membrane based cells. This trend is in very good agreement with the findings of Rice et al.[9] However in their case it was the membrane dehydration that resulted in the increase in cell resistance with increase in formic acid concentration. Since the cell considered in the present study is a membraneless one and formic acid is a very good electrolyte, the proportion of protons available for ionic transport is expected to increase with formic acid concentration. Furthermore, H_2SO_4 is also a very good proton conductor. The proton conductivity of 0.5 M H_2SO_4 is of the order of 0.2 S cm^{-2}, which is twice as that of Nafion at 100% relative humidity.[7] In calculating the cell impedance, it is assumed that a geometric surface area of 0.35 cm^2 of the graphite electrode is in contact with the

paper. However, the actual contact area will be much smaller after CO_2 bubble formation, and therefore the cell impedance will be smaller than that of the value calculated using the visible contact area. Since in the configuration used here, the paper strip is placed above the anode, it is not possible to observe the bubble formation. For a similar set up, Arun et al.[17] observed the formation of CO_2 bubbles at the anode. Therefore, the only reasoning here for the increase in cell resistance with formic acid concentration is the formation of tiny CO_2 bubbles, which reduces the contact area.

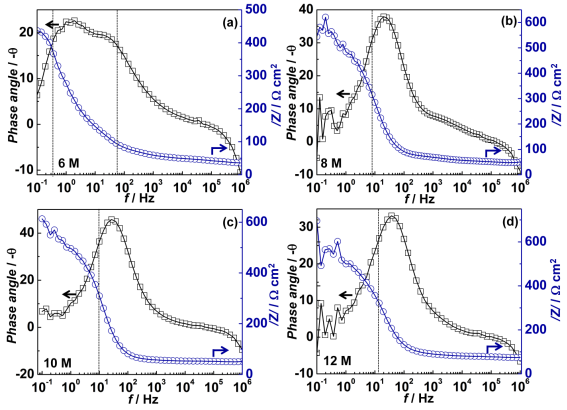

Figure 11: Bode diagram corresponding to the impedance curves given in Fig. Figure 8. The black dashed constant frequency lines correspond to the relaxation frequencies presented in Fig. Figure 8 for different values of concentration of formic acid.

The Bode diagrams corresponding to the impedance plots presented in Fig. Figure 8 are shown in Fig. Figure 11. In all cases, the phase angle, defined as $\theta = \tan^{-1}(Z_i/Z_r)$ is well below -45 degree indicating that the process can not be represented using a RC circuit. For a pure RC circuit, the phase angle reaches -45 degree at the characteristic frequency. For the concentration range of 8 M-12 M, at the characteristic frequency the phase angle varies between -25 to -35 degrees. For the cell with 6 M formic acid concentration, two relaxation frequencies are observed. In Fig. Figure 8(b)- Fig. Figure 8(d), it is observed that at high frequencies an inductance contribution is present over a small range, probably because of the lead, which makes the phase angle positive at the high frequency limit. The Bode diagram corresponding to Fig. Figure 9 is shown in Fig. Figure 12. The trend in phase angle at 0.77 V is very much similar to the cell's behavior at OCV. The phase angle is

-28 degree at the characteristic frequency and an inductance component is present at high frequency limit.

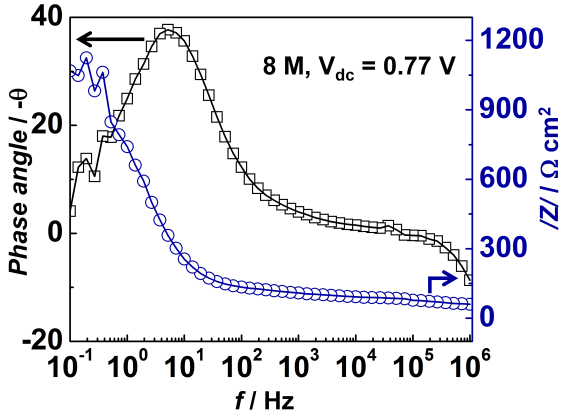

Figure 12: Bode diagram corresponding to the impedance curves given in Fig. Figure 9.

Concluding remarks

In this work, we have presented a low cost, environmentally friendly porous paper based fuel cell operating on formic acid (HCOOH) as the fuel and potassium permanganate ($KMnO_4$) as the oxidant. The oxidation of formic acid at the anode is achieved using a graphite sheet electrode without the use of any metal catalysts. Although the paper based fuel cell functions according to the principles of laminar flow fuel cells, fuel mixing can still occur due to the non-directionality associated with the cellulose fibres and hence the cell performance is largely dependent on the micro-structure of the filter paper.. In order to delay the fuel and oxidant cross over a slit is provided at the center of the paper strip. Although the slit delays the cross over effects, it also increases the Ohmic resistance of the cell due to the longer diffusion path for the ions to reach the cathode. In addition to the slit width the position of electrodes from the end of the slit also plays a major role in deciding the cell performance. Based on the slit width and the electrode position studies, for cell characterization the slit width is maintained at 4 mm the electrodes are placed at 1 cm away from the end of the slit. The best cell performance is obtained for 8 M formic

acid concentration, which is in close agreement with the observations made in other direct formic acid fuel cells. The cell with 8 M formic acid delivers an OCV of 1.3 V, with a maximum power density of 0.57 mW/cm^2 at 0.77 V. Several factors, such as fuel cross over, fuel and oxidant dilution contribute to the loss in OCV from its' theoretical value. Electrochemical impedance spectroscopic data analysis reveals that the kinetics of the cell is sluggish due to the slow oxidation kinetics of formic acid. Furthermore, for all formic acid concentrations, at the characteristic frequency the phase angle lies between -25 and -35 degrees indicating that the cells do not follow an ideal Randles circuit. The impedance response of the cell at 0.77 V resulted in higher polarization resistance, however, the phase angles was similar to that at OCV. Finally, the power delivered by the cell is sufficient to power MNSs whose power requirements are in the range of milli-watts to nano-watts. Our successful implementation of the $HCOOH-H_2SO_4-KMnO_4$ fuel cell at room temperature by using an over simplified paper based architecture opens up many opportunities to apply this configuration to yet unexplored alkali/methanol based fuel cell systems.

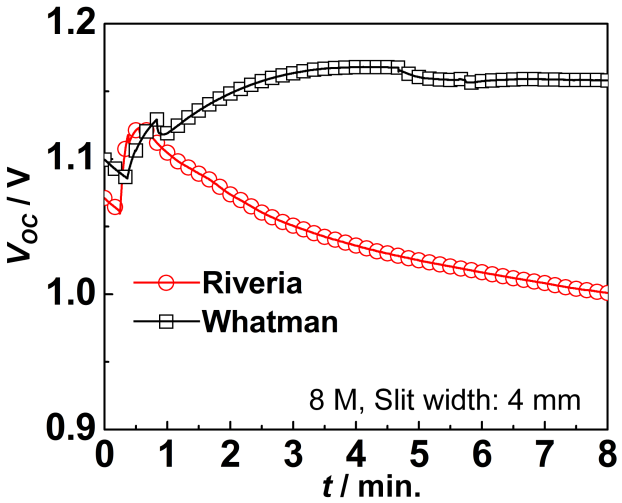

Figure S1: Open circuit voltage for generated by cells made of Whatmann and Riveria filter papers with 8M formic acid. The electrodes are placed 1 cm away from the end of the slit.

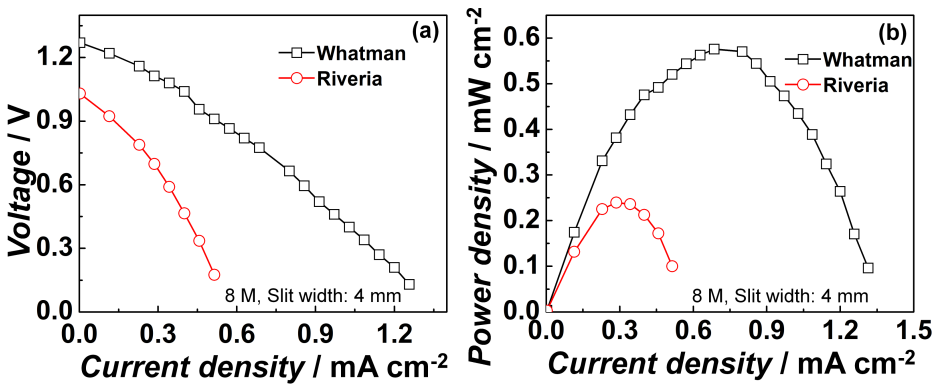

Figure S2: Performance comparison between cells made of Whatmann and Riveria filter papers using 8M formic acid. The electrodes are placed 1 cm away from the end of the slit.

References

[1] Wang, Z. L.; Wu, W. *Angew. Chem. Int. Ed* **2012**, *51*, 2–24.

[2] Fraiwan, A.; Mukherjee, S.; Sundermier, S.; Lee, H. S.; Choi, S. *Biosens. Bioelectron.* **2013**, *49*, 410–414.

[3] Wang, S.; Ge, L.; Zhang, Y.; Song, X.; Li, N.; Gea, S.; Yu, J. *Lab Chip* **2012**, *12*, 4489–4498.

[4] Esquivel, J. P.; Del Campo, F. J.; Gómez de la Fuente, J. L.; Rojas, S.; Sabaté, N. *Energy Environ. Sci* **2014**, *7*, 1744–1749.

[5] Yu, J.; Ge, L.; Huang, J.; Wang, S.; Gr, S. *Lab Chip* **2011**, *11*, 1286–1291.

[6] Chang, M.-h.; Chen, F.; Fang, N.-s. *J. Power Sources* **2006**, *159*, 810–816.

[7] Ali, S.; Shaegh, M.; Nguyen, N.-t.; Chan, S. H. *Int. J. Hydrog. Energy* **2011**, *36*, 5675–5694.

[8] Kreuer, K. D. *J. Membr. Sci.* **2001**, *185*, 29–39.

[9] Rice, C.; Ha, S.; Masel, R. I.; Waszczuk, P.; Wieckowski, A.; Barnard, T. *J. Power Sources* **2002**, *111*, 83–89.

[10] Zhu, Y.; Ha, S. Y.; Masel, R. I. *J. Power Sources* **2004**, *130*, 8–14.

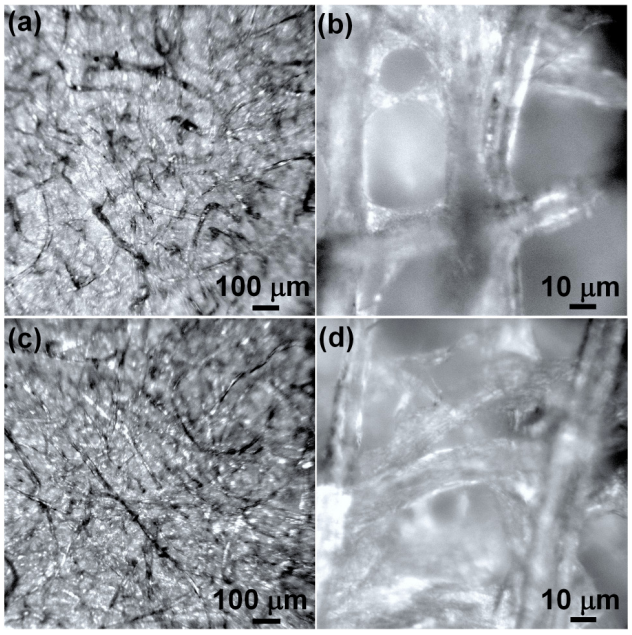

Figure S3: Optical microscope image of Whatman and Riveria filter paper. (a) and (b) shows Whatman and (c) and (d) shows Riveria.

[11] Ha, S.; Dunbar, Z.; Masel, R. *J. Power Sources* **2006**, *158*, 129–136.

[12] Jeon, M. K.; Won, J. Y.; Oh, K. S.; Lee, K. R.; Woo, S. I. *Electrochim. Acta* **2007**, *53*, 447–452.

[13] Chetty, R.; Scott, K. *J. New Mater. Electrochem. Syst.* **2007**, *142*, 135–142.

[14] Yu, X.; Pickup, P. G. *J. Power Sources* **2008**, *182*, 124–132.

[15] Tominaka, S.; Ohta, S.; Obata, H.; Momma, T.; Osaka, T. *J. Am. Chem. Soc.* **2008**, *130*, 10456–10457.

[16] Chiban, E. R.; Markoski, L. J.; Wieckowski, A.; Kenis, P. J. *J. Power Sources* **2004**, *128*, 54–60.

[17] Arun, R. K.; Halder, S.; Chanda, N.; Chakraborty, S. *Lab Chip* **2014**, *14*, 1661–1664.